

# Superfluid Mutual-friction Coefficients from Vortex Dynamics in the Two-dimensional Galerkin-truncated Gross-Pitaevskii Equation

Vishwanath Shukla,<sup>1,\*</sup> Marc Brachet,<sup>2,†</sup> and Rahul Pandit<sup>3,‡</sup>

<sup>1</sup>*Centre for Condensed Matter Theory, Department of Physics,  
Indian Institute of Science, Bangalore 560012, India*

<sup>2</sup>*Laboratoire de Physique Statistique de l'Ecole Normale Supérieure,  
associé au CNRS et aux Universités Paris VI et VII, 24 Rue Lhomond, 75231 Paris, France*

<sup>3</sup>*Centre for Condensed Matter Theory, Department of Physics,  
Indian Institute of Science, Bangalore 560012, India.*

(Dated: December 3, 2014)

We present algorithms for the ab-initio determination of the temperature ( $T$ ) dependence of the mutual-friction coefficients  $\alpha$  and  $\alpha'$  and the normal-fluid density  $\rho_n$  in the two-dimensional (2D) Galerkin-truncated Gross-Pitaevskii system. Our algorithms enable us to determine  $\alpha(T)$ , even though fluctuations in 2D are considerably larger than they are in 3D. We also examine the implications of our measurements of  $\alpha'(T)$  for the Iordanskii force, whose existence is often questioned.

PACS numbers: 67.25.dk, 47.37.+q, 67.25.dm, 67.25.D-  
Keywords: superfluid; turbulence; mutual-friction

The elucidation of the statistical properties of superfluid turbulence and the comparison of these with their fluid-turbulence analogs is a problem of central importance that lies at the interface between fluid dynamics and statistical mechanics [1, 2]. Theoretical treatments of superfluid turbulence use a variety of models [3–5], which are applicable at different length scales and for different interaction strengths. At low temperatures  $T$  and for weakly interacting bosons, the Gross-Pitaevskii (GP) equation provides a good hydrodynamical description of a superfluid with quantum vortices. If we consider length scales that are larger than the mean separation between quantum vortices, and if we concentrate on low-Mach-number flows, then the two-fluid model [6, 7] of Hall, Vinen, Bekharevich, and Khalatnikov (HVBK) provides a good description of superfluid turbulence. In the HVBK equations, the normal and superfluid velocities are coupled by two mutual-friction coefficients,  $\alpha$  and  $\alpha'$ . The determination of  $\alpha$  and  $\alpha'$ , along with the normal-fluid density  $\rho_n$ , as functions of  $T$ , from (a) experiments [6, 8, 9], (b) kinetic models [3, 5, 10], or (c) the Galerkin-truncated GP equation [11, 12] is a challenging problem. Such studies have been carried out only in three dimensions (3D). Given that (a) two-dimensional (2D) and 3D fluid turbulence are qualitatively different [13, 14] and (b) 2D and 3D superfluids are also qualitatively different [15, 16], it behooves us to carry out GP-based investigations of  $\alpha$  and  $\alpha'$  for a 2D superfluid.

We present the first calculation of  $\alpha(T)$ ,  $\alpha'(T)$ , and  $\rho_n(T)$  in the 2D Galerkin-truncated GP system. The de-

termination of  $\alpha(T)$ ,  $\alpha'(T)$ , and  $\rho_n(T)$  turns out to be considerably more challenging in 2D than in 3D [11] because of large fluctuations. We obtain the dependence of  $\alpha(T)$ ,  $\alpha'(T)$ , and  $\rho_n(T)$  on  $T$  by using an algorithm, which allows us to examine the evolution of vortical configurations, such as, a pair of vortices and a quadruplet of vortices, placed initially at the corners of a square. We find that  $\alpha'(T)$  is smaller than  $\alpha(T)$  in magnitude, but nonzero; this suggests that the Iordanskii force [17–23], whose existence has often been questioned, does not vanish.

The Galerkin-truncated GP equation for the complex, classical field  $\psi(\mathbf{x}, t)$  of a weakly interacting 2D Bose gas is

$$i\frac{\partial\psi(\mathbf{x}, t)}{\partial t} = \mathcal{P}_G \left[ -\alpha_0 \nabla^2 \psi(\mathbf{x}, t) + g \mathcal{P}_G[|\psi|^2] \psi(\mathbf{x}, t) \right], \quad (1)$$

where  $g$  is the effective interaction strength, the Galerkin projector  $\mathcal{P}_G[\hat{\psi}(k)] = \theta(k_{\max} - k) \hat{\psi}(k)$ , with  $\hat{\psi}$  the Fourier transform of  $\psi$  and  $\theta(\cdot)$  the Heaviside function. This truncated GP equation (TGPE) conserves the total energy  $H = 2\alpha_0 \int_{\mathcal{A}} d^2x (\alpha_0 |\nabla \psi|^2 + \frac{g}{2} [\mathcal{P}_G[|\psi|^2]]^2)$ , the total number of particles  $N = \int_{\mathcal{A}} d^2x |\psi|^2$ , and the momentum  $\mathbf{P} = \alpha_0 \int_{\mathcal{A}} d^2x (\psi \nabla \psi^* - \psi^* \nabla \psi)$ . The Madelung transformation  $\psi = \sqrt{\rho(\mathbf{x}, t)} \exp(i\phi)$ , where  $\rho$  and  $\phi$  are the density and phase field, respectively, yields the velocity  $\mathbf{v} = 2\alpha_0 \nabla \phi$ , with the quantum of circulation  $4\pi\alpha_0$ , the sound velocity  $c = \sqrt{g\rho^*}$ , the healing length  $\xi = \sqrt{2\alpha_0^2/(g\rho^*)}$ , the total density  $\rho^* = N/\mathcal{A}$ , and  $\mathcal{A} = L^2$  is the area of our 2D, periodic, computational domain of side  $L = 2\pi$  (see the Supplemental Material [24] for units). We use the 2/3 dealiasing rule in our pseudospectral direct numerical simulation (DNS) of the TGPE, with the maximum wave number  $k_{\max} = 2/3 \times N_c/2$ , where  $N_c$  is the number of collocation points [11]. This scheme ensures global-momentum conservation in our DNSs and it is essential for capturing accurately the interactions of the

\* research.vishwanath@gmail.com

† brachet@physique.ens.fr

‡ rahul@physics.iisc.ernet.in;

also at Jawaharlal Nehru Centre For Advanced Scientific Research, Jakkur, Bangalore, India.

normal fluid with the superfluid vortices [11]. We use a fourth-order, Runge-Kutta scheme, with time step  $\Delta t$ , for time marching.

Generic initial conditions evolve slowly, under the 2D TGPE dynamics, towards equilibrium in the microcanonical ensemble [12]: the system goes through initial transients, then displays the onset of thermalization, which is followed by a regime of partial thermalization, and then complete thermalization, with a low- $T$  Berezinskii-Kosterlitz-Thouless (BKT) phase, a high- $T$  phase with unbound vortices, and a transition between these phases at  $T_{\text{BKT}}$ . To accelerate equilibration and to have direct control over (a)  $T$ , for the desired equilibrium state, and (b) states with counterflows, we use the generalized grand canonical ensemble with the equilibrium probability distribution  $\mathbb{P}[\psi] = \Xi^{-1} \exp[-\beta(H - \mu N - \mathbf{w} \cdot \mathbf{P})]$ , where  $\Xi$  is the grand partition function,  $\beta = T^{-1}$  (we set the Boltzmann constant  $k_B = 1$ ),  $\mu$  the chemical potential,  $\mathbf{w} = \mathbf{v}_n - \mathbf{v}_s$  the counterflow velocity, and  $\mathbf{v}_n$  and  $\mathbf{v}_s$  the normal and superfluid velocities, respectively. We construct a stochastic process, which leads to this  $\mathbb{P}[\psi]$ , via the 2D stochastic Ginzburg-Landau equation (SGLE)

$$\frac{\partial \psi}{\partial t} = \mathcal{P}_G \left[ \alpha_0 \nabla^2 \psi - g \mathcal{P}_G[|\psi|^2] \psi + \mu \psi - i \mathbf{w} \cdot \nabla \psi + \zeta(\mathbf{x}, t) \right], \quad (2)$$

where  $\zeta$  is a zero-mean, Gaussian white noise with  $\langle \zeta(\mathbf{x}, t) \zeta^*(\mathbf{x}', t') \rangle = D \delta(\mathbf{x} - \mathbf{x}') \delta(t - t')$ ,  $\delta$  the Dirac delta function, and  $D = 1/(2\alpha\beta)$ , in accordance with the fluctuation-dissipation theorem. We solve this SGLE along with

$$\frac{d\mu}{dt} = -\frac{\nu_N}{\mathcal{A}} (N - N_{av}), \quad (3)$$

so that  $N_{av}$  controls the mean value of  $N$  and  $\nu_N$  governs the rate at which the SGLE equilibrates. The counterflow term  $i \mathbf{w} \cdot \nabla \psi$  yields states with a non-vanishing  $\mathbf{w}$ .

In the HVBK model [6, 8, 25], a superfluid vortex does not move with the superfluid velocity  $\mathbf{v}_s$  but with velocity

$$\mathbf{v} = \mathbf{v}_{sl} + \alpha \mathbf{s}' \times (\mathbf{v}_n - \mathbf{v}_{sl}) - \alpha' \mathbf{s}' \times [\mathbf{s}' \times (\mathbf{v}_n - \mathbf{v}_{sl})], \quad (4)$$

where  $\mathbf{v}_{sl} = \mathbf{v}_s + \mathbf{v}_{si}$  is the local superfluid velocity, with  $\mathbf{v}_s$  and  $\mathbf{v}_{si}$  the imposed superfluid velocity and the self-induced velocity because of the vortices, respectively, and  $\mathbf{s}'$  the unit tangent at a point on the vortex, with position vector  $\mathbf{s}$  [26]. We use the following two initial configurations in the 2D TGPE: (1)  $\psi_{\text{IC1}} = \psi_{\text{pair}} \psi_{\text{eq}}$ ; and (2)  $\psi_{\text{IC2}} = \psi_{\text{lattice}} \psi_{\text{eq}}^{\text{cf}}$ . We obtain  $\psi_{\text{IC1}}$  by (a) first preparing a state  $\psi_{\text{pair}}$ , which corresponds to a small, vortex-antivortex pair translating with a constant velocity along the  $x$  direction (Supplemental Material [24]) and (b) then combining it with an equilibrium state  $\psi_{\text{eq}}$  to include finite-temperature effects (Supplemental Material [24]). To obtain  $\psi_{\text{IC2}}$ , we first prepare  $\psi_{\text{lattice}}$ , in which we place vortices of alternating signs on the corners of a square (a vortex lattice by virtue of the periodic boundary conditions) (Supplemental Material [24]); and then we include finite-temperature and counterflow effects by multiplying

	$T/\tilde{T}_{\text{BKT}}$	$\rho_n$	$\alpha_{\text{IC1}}$	$\mathbf{w}$	$\alpha_{\text{IC2}}$	$\alpha'_{\text{IC2}}$
R1	$6.37 \times 10^{-4}$	$2.7 \times 10^{-4}$	$(2 \pm 1) \times 10^{-6}$	$0.8 \ 2.5 \times 10^{-5}$	$-2.2 \times 10^{-5}$	
R2	$3.19 \times 10^{-3}$	$1.37 \times 10^{-3}$	$(1.0 \pm .3) \times 10^{-4}$	$0.8 \ 1.8 \times 10^{-4}$	$-1.5 \times 10^{-4}$	
R3	$6.37 \times 10^{-3}$	$2.7 \times 10^{-3}$	$(2.2 \pm .6) \times 10^{-4}$	$0.6 \ 3.6 \times 10^{-4}$	$-1.8 \times 10^{-4}$	
R4	$3.19 \times 10^{-2}$	$1.39 \times 10^{-2}$	$(1.6 \pm .5) \times 10^{-3}$	$0.4 \ 2.3 \times 10^{-3}$	$-4.5 \times 10^{-4}$	
R5	$6.37 \times 10^{-2}$	$2.85 \times 10^{-2}$	$(4 \pm 1) \times 10^{-3}$	$0.2 \ 6.9 \times 10^{-3}$	$4.0 \times 10^{-4}$	
R6	$9.56 \times 10^{-2}$	$4.37 \times 10^{-2}$	—	$0.1 \ 1.2 \times 10^{-2}$	$-1.2 \times 10^{-3}$	
R7	$1.20 \times 10^{-1}$	$5.97 \times 10^{-2}$	$(1.2 \pm .6) \times 10^{-2}$	$0.1 \ 1.6 \times 10^{-2}$	$2.9 \times 10^{-3}$	
R8	$1.59 \times 10^{-1}$	$7.66 \times 10^{-2}$	—	$0.1 \ 1.4 \times 10^{-2}$	$4.2 \times 10^{-3}$	
R9	$1.78 \times 10^{-1}$	$8.71 \times 10^{-2}$	—	$0.1 \ 2.2 \times 10^{-2}$	$-3.5 \times 10^{-3}$	

TABLE I. Mutual-friction results from our DNS runs R1-R9:  $T/\tilde{T}_{\text{BKT}}$  is the scaled temperature;  $\tilde{T}_{\text{BKT}} = 1.57 \times 10^{-2}$  is the energy-entropy-argument based estimate of the BKT transition temperature;  $\rho_n$  is the normal-fluid density;  $\mathbf{w} = v_n \hat{x}$  is the counterflow velocity;  $\alpha$  and  $\alpha'$  are the mutual friction coefficients, where the subscripts IC1 and IC2 denote the initial configurations. In all our DNS runs, the total average density  $\rho^* = N/\mathcal{A} = 1$ , the total number of collocation points  $N_c^2 = 128^2$ , the healing length  $\xi = 1.44\Delta x$ ,  $\Delta x = 2\pi/N_c$ , the speed of sound  $c = 1$ , and the quantum of circulation  $\alpha_0 \simeq 0.05$  are kept fixed.

$\psi_{\text{lattice}}$  with the state  $\psi_{\text{eq}}^{\text{cf}}$  (Supplemental Material [24]). We obtain  $\psi_{\text{eq}}$  and  $\psi_{\text{eq}}^{\text{cf}}$  by solving the SGLE (2); and then we use  $\psi_{\text{IC1}}$  to determine  $\alpha(T)$  and  $\psi_{\text{IC2}}$  to calculate both  $\alpha(T)$  and  $\alpha'(T)$ .

Our DNS of the TGPE Eq. (1) yields the spatiotemporal evolutions of  $\psi_{\text{IC1}}$  and  $\psi_{\text{IC2}}$ . We take  $\mathbf{w} = v_n \hat{x}$  for all our SGLE DNSs with counterflows. Parameters for our DNSs are summarized in Table I. We first plot the  $x$  component of the momentum  $P_x$  versus  $v_n$ , for five representative values of  $T/\tilde{T}_{\text{BKT}}$  (Fig. 1(a)), whence we obtain

$$\rho_n(T) = \frac{1}{\mathcal{A}} \frac{\partial P_x}{\partial v_n} \Big|_{v_n=0}, \quad (5)$$

whose values we list in column 3 of Table I. In Fig. 1(b), we plot, versus the scaled temperature  $T/\tilde{T}_{\text{BKT}}$ , where  $\tilde{T}_{\text{BKT}}$  is a rough, energy-entropy-argument estimate of the BKT transition temperature [15, 16],  $\rho_n$  (green curve),  $(1 - \rho_n)$  (sky-blue curve), and the condensate fraction  $N_0/N$  (purple line), where  $N_0$  is the population of the zero-wave-number mode.

We begin with our results for the spatiotemporal evolution of  $\psi_{\text{IC1}} = \psi_{\text{pair}} \psi_{\text{eq}}$ . The vortex-antivortex pair in  $\psi_{\text{pair}}$ , have centers that are separated, initially, by the small distance  $d(t=0) \simeq 5.4\xi$  in the  $y$  direction; the pair moves at a constant velocity  $v_{\text{pair}} = 0.2775\hat{x}$ . The state  $\psi_{\text{eq}}$ , which is an absolute-equilibrium state at a temperature  $T < T_{\text{BKT}}$ , provides the normal fluid that interacts with this vortex-antivortex pair and leads to a decrease in  $d$  as time increases. In the Supplemental Material [24] we show that

$$dd^2/dt = -8\alpha_0(1 - \alpha')\alpha; \quad (6)$$

we can neglect  $\alpha'$  here (as we show below,  $\alpha' \ll 1$ ). Thus, we can obtain  $\alpha(T)$  from the slope of a straight-line fit

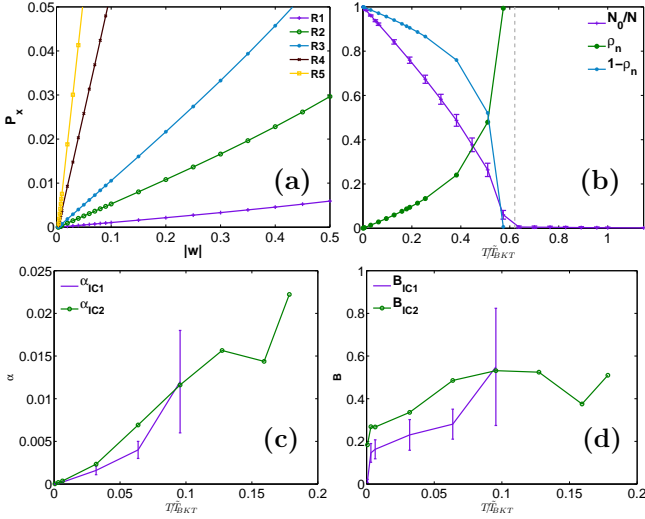


FIG. 1. (Color online) Plots of (a) the momentum  $P_x$  versus the applied counterflow velocity  $w$  for the DNS runs R1-R5; (b) the condensate fraction  $N_0/N$  (purple line), the normal fluid density  $\rho_n$  (green line), and  $1 - \rho_n$  (sky-blue line) versus  $T/\tilde{T}_{BKT}$ ; (c) the mutual friction coefficients  $\alpha_{IC1}$  (purple line) and  $\alpha_{IC2}$  (green line) versus  $T/\tilde{T}_{BKT}$ ; (d)  $B = 2\alpha/\rho$  versus  $T/\tilde{T}_{BKT}$ . Here the subscripts on  $\alpha$  refer to the initial conditions IC1 and IC2.

to a plot of  $d^2$  versus  $t$ . We determine  $d^2(t)$  by tracking the positions of the vortices and thus obtain plots such as those shown in Fig. 2 for two representative values of  $T/\tilde{T}_{BKT}$  (DNS runs R2 and R4 in Table I). The Video M1, for the DNS run R2, shows, via pseudocolor plots, the spatiotemporal evolution of the field  $|\psi(\mathbf{x}, t)|^2$ : the vortex-antivortex pair moves under the combined influence of its initial momentum and the finite-temperature fluctuations, the average value of  $d$  decreases with time and, finally, this pair disappears from the system (on time scales that are much longer than those shown in this video). From the plots in Fig. 2 we see that (a)  $d^2$  fluctuates significantly in time and (b) these fluctuations increase with  $T/\tilde{T}_{BKT}$  (compare Figs. 2(a) and (b)). Thus, the higher the temperature, the more these fluctuations limit our ability to determine  $d^2$  reliably, with averages over a fixed number of realizations of  $\psi_{eq}$ , which we must limit, perforce, because of the computational cost of these calculations. We obtain 10 values of  $\alpha(T)$ , because we use 10 realizations of  $\psi_{eq}$ . The mean of these values yield the value of  $\alpha(T)$  that we have listed in column 4 of Table I; the standard deviations yield the error bars;  $\alpha$  increases with  $T$  (over the range we consider).

The state  $\psi_{lattice}$  consists of a quadruplet of alternating vortices and antivortices on the vertices of a square with sides of length  $\pi$ ; for this state, the self-induced velocity  $\mathbf{v}_{si}$ , because of these vortices and antivortices, is zero at  $T = 0$ . In  $\psi_{IC2}$  we combine  $\psi_{lattice}$  with the thermalized state  $\psi_{eq}^{cf}$ , at different values of  $T/\tilde{T}_{BKT}$  and counterflow velocity  $\mathbf{w} = v_n \hat{x}$ . Figures 3(a) and (b) show pseudocolor plots of the density field, for our DNS run

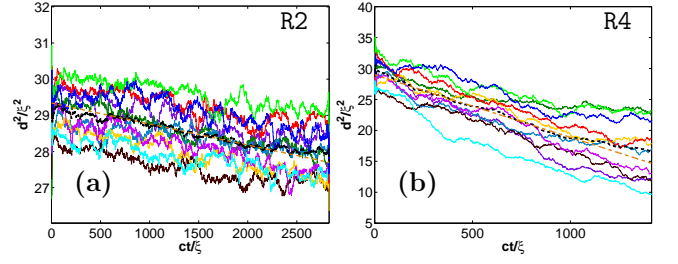


FIG. 2. (Color online) Plots of the square of the vortex-pair length  $d^2/\xi^2$  versus time  $ct/\xi$  from our DNS runs: (a) R2 at  $T/\tilde{T}_{BKT} = 3.19 \times 10^{-3}$ ; (b) R4 at  $T/\tilde{T}_{BKT} = 3.19 \times 10^{-2}$ . For each plot, the different solid lines indicate the time evolution of  $d^2/\xi^2$  for the different realizations of  $\psi_{eq}$ , which we obtain from the steady state of the SGLE. To reduce the noise in the plots of  $d^2$ , for these different realizations we have used a moving-average-based smoothing procedure (the function *smooth* in Matlab®); this procedure introduces slight artifacts (high or low values of  $d^2$ ) near the lowest and highest values of  $t$  in these plots. To obtain  $\alpha(T)$ , we use the average of all the plots of  $d^2$  versus  $t$  (dashed black curve), at given value of  $T$ . The orange dashed line, a linear fit to this curve, is shown to guide the eye.

R2 at  $T/\tilde{T}_{BKT} = 3.19 \times 10^{-3}$  and  $v_n = 0.8$ , at two different times  $t = 0$  and  $t = 1000$ . Figures 3(a) and (b) and the corresponding Video M2 show that the vortex lattice drifts under the influence of the imposed counterflow. Initially the vortex-lattice has an adaptation time period, during which a perpendicular motion, with a negligibly small velocity, and a drift, parallel to the applied counterflow, yield a vortex lattice imperfection, which we quantify by  $\delta = \frac{1}{4}[(\delta y_2 + \delta y_4) - (\delta y_1 + \delta y_3)]$ , where  $\delta y_i$  is the  $y$ -displacement of the vortex  $i$  (see Fig. 4(a) inset); the drift parallel to the applied counterflow is given by  $\delta x = \frac{1}{4}(\delta x_1 + \delta x_2 + \delta x_3 + \delta x_4)$ , with  $\delta x_i$  the  $x$ -displacement of the vortex  $i$ . The imperfection  $\delta(t)$  increases with  $t$  and results in a self-induced velocity  $\mathbf{v}_{si}$ , which leads to a decrease in the effective counterflow  $w(t)$  because of the conservation of the total momentum. We develop a phenomenological model, which accounts for this effect (Supplemental Material [24]) and yields

$$\delta(t) = \frac{\rho_n w_0}{\alpha_0(\chi_v \rho_n + \chi_p \rho)} \left( 1 - \exp\left[-\frac{\alpha \alpha_0(\chi_v \rho_n + \chi_p \rho)}{\rho_n} t\right] \right) \quad (7)$$

and

$$\begin{aligned} \delta x(t) = & \left( [\chi_v \rho_n - \alpha'(\chi_v \rho_n + \chi_p \rho)] \times \right. \\ & \left. \exp\left[-\frac{\alpha \alpha_0(\chi_v \rho_n + \chi_p \rho)}{\rho_n} t\right] - \chi_v \rho_n \right. \\ & \left. + (\chi_v \rho_n + \chi_p \rho)(\alpha' + \alpha \alpha_0 t) \right) \frac{\rho_n w_0}{\alpha \alpha_0(\chi_v \rho_n + \chi_p \rho)^2}, \end{aligned} \quad (8)$$

where  $w_0$  is the counterflow velocity at  $t = 0$ ;  $\chi_v$  and  $\chi_p$  are the proportionality constants given by  $v_{si}(\delta) = \chi_v \alpha_0 \delta$

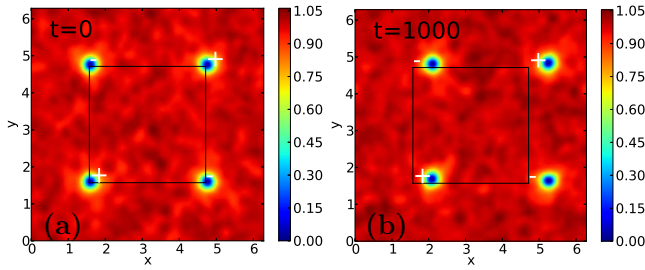


FIG. 3. (Color online) Pseudocolor plots of the density field  $|\psi(\mathbf{x}, t)|^2$  from our DNS run R2 at two different instants of time: (a)  $t = 0$  and (b)  $t = 1000$ ; these show the drift of the vortex crystal under the imposed counterflow  $v_n = 0.8\hat{x}$  at  $T/\tilde{T}_{\text{BKT}} = 3.19 \times 10^{-3}$ . The + and - symbols (in white) show the signs of the vortices; and the black frame indicates the square at whose corners we place  $\pm$  vortices at  $t = 0$ . The Video M2 shows, via pseudocolor plots, the spatiotemporal evolution of  $|\psi(\mathbf{x}, t)|^2$ .

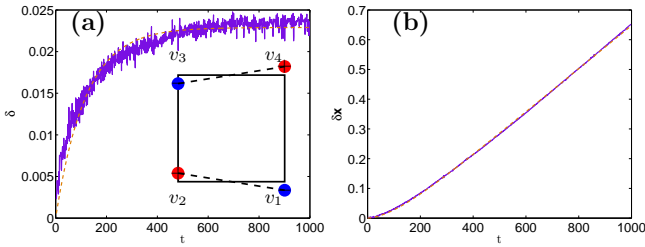


FIG. 4. (Color online) Plots versus time  $t$  of (a) the imperfection  $\delta = \frac{1}{4}[(\delta y_2 + \delta y_4) - (\delta y_1 + \delta y_3)]$  and (b) the drift  $\delta x = \frac{1}{4}(\delta x_1 + \delta x_2 + \delta x_3 + \delta x_4)$ , from our DNS run R2. The orange-dashed lines indicate the fits obtained by the use of Eqs. (7) and (8) (see text). Inset: a schematic diagram of the vortex-lattice imperfection; the square shows the shape of the vortex lattice at  $t = 0$ .

and  $P_{\text{si}}(\delta) = 4\pi^2 \chi_P \alpha_0 \rho \delta$ , where  $P_{\text{si}}$  is the self-induced momentum from the vortex-lattice imperfection. We determine  $\alpha(T)$  and  $\alpha'(T)$  from the fits, suggested by the forms in Eqs. (7) and (8), to the plots of  $\delta$  and  $\delta x$ , which we obtain from our DNS runs R1-R9 at different temperatures [details in the Supplemental Material [24]]. Figures 4(a) and (b) contain plots versus  $t$  of  $\delta(t)$  and  $\delta x(t)$ , respectively; Fig. 4(a) shows the saturation, at large  $t$ , of the vortex-lattice imperfection. The values of  $\alpha(T)$  and  $\alpha'(T)$  that we obtain are listed in columns 6 and 7 of Table I for different values of  $T/\tilde{T}_{\text{BKT}}$ . It is reassuring to note that the values we obtain for  $\alpha(T)$  from configurations IC1 and IC2 (columns 4 and 6) agree with each other.

The measurement of  $\alpha'(T)$  in 2D is difficult because of the following reasons: (1) at low temperatures its magnitude is small; (2) at high temperatures there are large thermal fluctuations that lead to large and noisy oscillations of the vortex lattice. Even though an accurate determination of  $\alpha'(T)$  is difficult, we find that  $\alpha'(T)$  is always nonzero and smaller in magnitude than  $\alpha(T)$ .

For similar studies in the 3D GPE we refer readers to Refs. [11, 27, 28]. In particular, Ref. [29] has studied  $\alpha(T)$  and  $\alpha'(T)$  in a pancake-type condensate.

We have shown how to obtain  $\alpha(T)$ ,  $\alpha'(T)$ , and  $\rho_n(T)$ , for 2D superfluids, by using the 2D Galerkin-truncated GP system. Even though the determination of  $\alpha(T)$ ,  $\alpha'(T)$ , and  $\rho_n(T)$  is difficult, we succeed in calculating them for  $T/\tilde{T}_{\text{BKT}} \lesssim 10^{-1}$ . At such low temperatures, the difference between the superfluid density  $\rho_s$ , which should be obtained strictly by using a helicity modulus [15, 16, 30], and  $(1 - \rho_n)$  should not be significant in typical, laboratory-scale systems; and the HVBK model, with the values of  $\alpha(T)$ ,  $\alpha'(T)$ , and  $\rho_n(T)$  that we have listed in Table I, should provide a good description of the dynamics of 2D superfluids so long as we probe scales that are larger than the mean separation between quantum vortices. The existence of the Iordanskii force, which is related to the third term on the right-hand side of Eq.(4), has been the subject of a debate in the latter half of the 1990s [17–23]. This force is linked to the asymmetry of the scattering of quasiparticles by a vortex [31, 32]; and, if it is present, it implies that  $\alpha'$  is nonzero. Thus, given that we find  $\alpha' \neq 0$ , our calculations imply that there is a nonvanishing Iordanskii force. To settle conclusively the issue of the existence of the Iordanskii force, we must obtain error bars on  $\alpha'(T)$ ; given the large fluctuations we have mentioned, the computational cost of obtaining such error bars is prohibitively large. We hope our study will lead to experimental measurements of  $\alpha(T)$ ,  $\alpha'(T)$ , and  $\rho_n(T)$  in 2D superfluids, whose analogs for 3D superfluids [8] have been known for several decades.

## ACKNOWLEDGEMENTS

We thank CSIR, UGC, DST (India) and the Indo-French Centre for Applied Mathematics (IFCAM) for financial support, and SERC (IISc) for computational resources. VS and RP thank ENS, Paris for hospitality and MB thanks IISc, Bangalore for hospitality.

## SUPPLEMENTAL MATERIAL

In this Supplemental Material we give, in Sec. I, video captions for the videos M1 and M2. Section II is devoted to the methods we use to determine  $\alpha$  and  $\alpha'$  from our DNSs. Section III contains a note on the units. Section IV describes the advective real Ginzburg-Landau equation (ARGLE). Section V gives an overview of the Stochastic-Ginzburg-Landau equation (SGLE) that we use. In Sections VI and VII we generalize standard results for the low-temperature phase of the Galerkin-truncated Gross-Pitaevskii equation by including a counterflow term.



## I. VIDEO CAPTIONS

**Video M1**(<http://youtu.be/yUxRhLDeGcI>): This video illustrates the spatiotemporal evolution of the field  $|\psi(\mathbf{x}, t)|^2$  for the initial configuration  $\psi_{\text{IC1}} = \psi_{\text{pair}}\psi_{\text{eq}}$  from our DNS run R2.

**Video M2**([http://youtu.be/gMp\\_Rj\\_aMns](http://youtu.be/gMp_Rj_aMns)): This video illustrates the spatiotemporal evolution of the field  $|\psi(\mathbf{x}, t)|^2$  for the initial configuration  $\psi_{\text{IC2}} = \psi_{\text{lattice}}\psi_{\text{eq}}^{\text{cf}}$  from our DNS run R2.

## II. MUTUAL FRICTION COEFFICIENTS $\alpha$ AND $\alpha'$

### A. Determination of $\alpha$ by using the initial configuration IC1

We can use Eq. (4) in the main paper to write the distance  $L_{\text{pair}}(t)$  travelled in the  $x$  direction by a vortex-antivortex pair of size  $d$  (in the  $y$  direction) as

$$\frac{dL_{\text{pair}}}{dt} = (1 - \alpha')v_{\text{si}} = (1 - \alpha')\frac{\kappa}{2\pi d}, \quad (9)$$

where  $\kappa = 4\pi\alpha_0$ . The time variation of  $d$  is governed by

$$\frac{dd}{dt} = -2\alpha\frac{dL_{\text{pair}}}{dt}, \quad (10)$$

where  $\alpha$  and  $\alpha'$  are the coefficients of mutual friction. Equations (9) and (10) yield

$$\frac{dd}{dt} = -4\alpha_0(1 - \alpha')\alpha\frac{1}{d}; \quad (11a)$$

$$\frac{dd^2}{dt} = -8\alpha_0(1 - \alpha')\alpha. \quad (11b)$$

Therefore,

$$\alpha = \frac{dd^2/dt}{8\alpha_0(1 - \alpha')} \approx \alpha = \frac{dd^2/dt}{8\alpha_0} \quad (12)$$

if  $\alpha' \ll 1$ .

### B. Determination of $\alpha$ and $\alpha'$ by using the initial configuration IC2

To a first approximation, the self-induced velocity  $v_{\text{si}}$  and momentum  $P_{\text{si}}$  are linear functions of the vortex-lattice imperfection  $\delta$ :

$$v_{\text{si}}(\delta) = \chi_v\alpha_0\delta; \quad (13)$$

and

$$P_{\text{si}}(\delta) = 4\pi^2\chi_P\alpha_0\rho\delta; \quad (14)$$

here  $\rho$  is the total density. The coefficients  $\chi_v$  and  $\chi_P$  depend on the properties of the system. We determine these by imposing a flow with velocity  $v_{\text{si}}$  on the perfect vortex lattice and then obtaining the ground state of this system by using the ARGLE coupled with a Newton's method (see Sec. IV); the vortex lattice adapts to the applied flow. We repeat the above procedure for different flow velocities and measure the imperfection  $\delta$  and the momentum  $P_{\text{si}}$ . The coefficients  $\chi_v$  and  $\chi_P$  are then extracted from the slopes of the linear fits to the plots of  $v_{\text{si}}$  versus  $\delta$  and  $P_{\text{si}}$  versus  $\delta$ , respectively (Eqs.(13) and (14)).

From Eq. (5) in the main paper the counterflow momentum

$$P_{\text{cf}}(w) = \rho_n w \mathcal{A}, \quad (15)$$

where  $\mathcal{A} = 4\pi^2$ . Total-momentum conservation implies that an increase in the vortex-lattice imperfection  $\delta$  leads to a decrease in the effective counterflow velocity  $w(\delta)$ . We have

$$P_0 = 4\pi^2\rho_n w_0 = P_{\text{si}} + P_{\text{cf}}, \quad (16)$$

where  $\rho_n$  is the normal-fluid density and  $P_0$  and  $w_0$  are the  $t = 0$  values of the counterflow momentum and velocity, respectively. Therefore, the counterflow velocity as a function of  $\delta$  is

$$w(\delta) = w_0 - \frac{\chi_P\alpha_0\rho}{\rho_n}\delta. \quad (17)$$

From Eq. (4) in the main paper the components of the velocity (for any vortex or antivortex in our system) parallel (||) and perpendicular ( $\perp$ ) to the counterflow velocity are, respectively,

$$\begin{aligned} v^{\parallel} &= v_{\text{si}}(\delta) + \alpha'[w(\delta) - v_{\text{si}}(\delta)] \\ &= \alpha_0\left(\chi_v - \alpha'\chi_v - \frac{\alpha'\chi_P\rho}{\rho_n}\right)\delta + \alpha'w_0 \end{aligned} \quad (18)$$

and

$$\begin{aligned} v^{\perp} &= \alpha[w(\delta) - v_{\text{si}}(\delta)] \\ &= \alpha w_0 - \frac{\alpha(\chi_v\rho_n + \chi_P\rho)\alpha_0}{\rho_n}\delta. \end{aligned} \quad (19)$$

The imperfection in the vortex lattice saturates when  $v^{\perp}$  is zero, which gives the following values for the imperfection and the drift velocity, respectively, at saturation (subscript  $\infty$ ):

$$\delta_{\infty} = \frac{\rho_n w_0}{\alpha_0(\chi_v\rho_n + \chi_P\rho)}; \quad (20)$$

and

$$v_{\infty}^{\parallel} = \frac{\chi_v\rho_n w_0}{\chi_v\rho_n + \chi_P\rho}. \quad (21)$$

The Eqs. (20) and (21) show that the large-time behavior of  $\delta$  and  $v''$  are independent of  $\alpha'$ . The equation of motion for  $\delta$  is

$$\frac{d\delta(t)}{dt} = \alpha w_0 - \frac{\alpha\alpha_0(\chi_v\rho_n + \chi_p\rho)}{\rho_n}\delta, \quad (22)$$

whose solution, with the initial condition  $\delta(0) = 0$ , is

$$\delta(t) = \frac{\rho_n w_0}{\alpha_0(\chi_v\rho_n + \chi_p\rho)} \left( 1 - \exp\left[-\frac{\alpha\alpha_0(\chi_v\rho_n + \chi_p\rho)}{\rho_n}t\right] \right). \quad (23)$$

We use Eq. (23) to rewrite Eq. (18) as

$$v''(t) = \frac{\chi_v\rho_n w_0}{\chi_v\rho_n + \chi_p\rho} + \left( \alpha' w_0 - \frac{\chi_v\rho_n w_0}{\chi_v\rho_n + \chi_p\rho} \right) \times \exp\left[-\frac{\alpha\alpha_0(\chi_v\rho_n + \chi_p\rho)}{\rho_n}t\right]; \quad (24)$$

the equation of motion for the drift  $\delta x$  is

$$\frac{d\delta x}{dt} = v_L''(t); \quad (25)$$

the solution of Eq. (25), with the initial condition  $\delta x(0) = 0$ , is

$$\begin{aligned} \delta x(t) = & \left( [\chi_v\rho_n - \alpha'(\chi_v\rho_n + \chi_p\rho)] \times \right. \\ & \exp\left[-\frac{\alpha\alpha_0(\chi_v\rho_n + \chi_p\rho)}{\rho_n}t\right] - \chi_v\rho_n \\ & \left. + (\chi_v\rho_n + \chi_p\rho)(\alpha' + \alpha\alpha_0 t) \right) \frac{\rho_n w_0}{\alpha\alpha_0(\chi_v\rho_n + \chi_p\rho)^2}. \end{aligned} \quad (26)$$

To extract  $\alpha$  and  $\alpha'$  from our data, from the DNS runs R1-R9 with the initial configuration IC2, we rewrite Eqs. (23) and (26), respectively, in the following simplified forms:

$$\delta(t) = D(1 - \exp(-Bt)) \quad (27)$$

and

$$\delta x(t) = A(1 - \exp(-Bt)) + Ct. \quad (28)$$

The coefficients are

$$A = \frac{\alpha'\rho_n w_0}{\alpha\alpha_0(\chi_p\rho + \chi_v)} - \frac{\chi_v\rho_n^2 w_0}{\alpha\alpha_0(\chi_p\rho + \chi_v)^2}, \quad (29)$$

$$B = \frac{\alpha\alpha_0(\chi_p\rho + \chi_v)}{\rho_n}, \quad (30)$$

$C = v_\infty''$ , and  $D = \delta_\infty$ . In Fig. 5(a) we compare the values of  $\delta_\infty$  and  $v_\infty''$ , obtained from fits to our DNS data, and the predictions of our phenomenological model (Eqs. (20) and (21)). Figure 5(b) shows the temperature variation of  $\alpha'$ . We cannot fit this reliably to any functional form; however, we can infer that  $\alpha'$  is smaller than  $\alpha$  in magnitude.

### III. NOTE ON UNITS

The GP equation, which describes the dynamical evolution of the wave function  $\psi(\mathbf{x}, t)$  of a weakly interacting, 2D Bose gas at low temperatures, is

$$i\hbar \frac{\partial \psi(\mathbf{x}, t)}{\partial t} = -\frac{\hbar^2}{2m} \nabla^2 \psi(\mathbf{x}, t) - \tilde{\mu} \psi(\mathbf{x}, t) + g_{2D} |\psi|^2 \psi(\mathbf{x}, t), \quad (31)$$

where  $g_{2D}$  is the effective interaction strength. As we have mentioned earlier, the GP equation conserves the energy, given by the Hamiltonian

$$H = \int_{\mathcal{A}} d^2x \left( \frac{\hbar^2}{2m} |\nabla \psi|^2 + g_{2D} |\psi|^4 \right), \quad (32)$$

and the total number of particles  $N = \int_{\mathcal{A}} d^2x |\psi|^2$ . We can use the Madelung transformation to write  $\psi(\mathbf{x}, t) = \sqrt{\rho(\mathbf{x}, t)/m} e^{i\phi(\mathbf{x}, t)}$ . The total density is  $\rho^* = N/\mathcal{A}$ . To obtain Eq.(1) in the main paper, we first divide Eq. (31) by  $\hbar$  and define  $\mu = \tilde{\mu}/\hbar$ ,  $g = g_{2D}/\hbar$ ; we then set  $\hbar/2m = \alpha_0$ , with  $m = 1$ . In these units, the quantum of circulation is  $\hbar/m = 4\pi\alpha_0$ , the sound velocity is  $c = \sqrt{g|\psi_0|^2/m} = \sqrt{g\rho_0}$ , and the healing length is  $\xi = \sqrt{\hbar^2/2m|\psi_0|^2g} = \sqrt{2\alpha_0^2/\rho_0g}$ , where  $\rho_0 = m|\psi_0|^2$  is the condensate density.

### IV. ADVECTIVE REAL GINZBURG-LANDAU EQUATION (ARGLE)

Compressible superfluid hydrodynamics, which is described by the GP equation, can lead, in the presence of vortices, to regimes dominated by acoustic emissions. To minimize these acoustic emissions, we prepare our initial states by using a specialized scheme, which we refer to as the advective-real-Ginzburg-Landau equation (ARGLE) [33]. The desired initial states are the large-time-asymptotic solutions of the ARGLE

$$\frac{\partial \psi}{\partial t} = \alpha_0 \nabla^2 \psi - g |\psi|^2 \psi + \mu \psi - i \mathbf{u}_{\text{adv}} \cdot \nabla \psi - \frac{\mathbf{u}_{\text{adv}}^2}{4\alpha_0} \psi; \quad (33)$$

and these states minimize the free-energy functional

$$\begin{aligned} \mathcal{F}_{\text{ARGLE}}(\psi, \psi^*) = & \int d^3x \left( \alpha_0 \left| \nabla \psi - i \frac{\mathbf{u}_{\text{adv}}}{2\alpha_0} \psi \right|^2 + \frac{1}{2} g |\psi|^4 \right. \\ & \left. - \mu |\psi|^2 \right); \end{aligned} \quad (34)$$

$\mathbf{u}_{\text{adv}}$  is the imposed flow velocity.

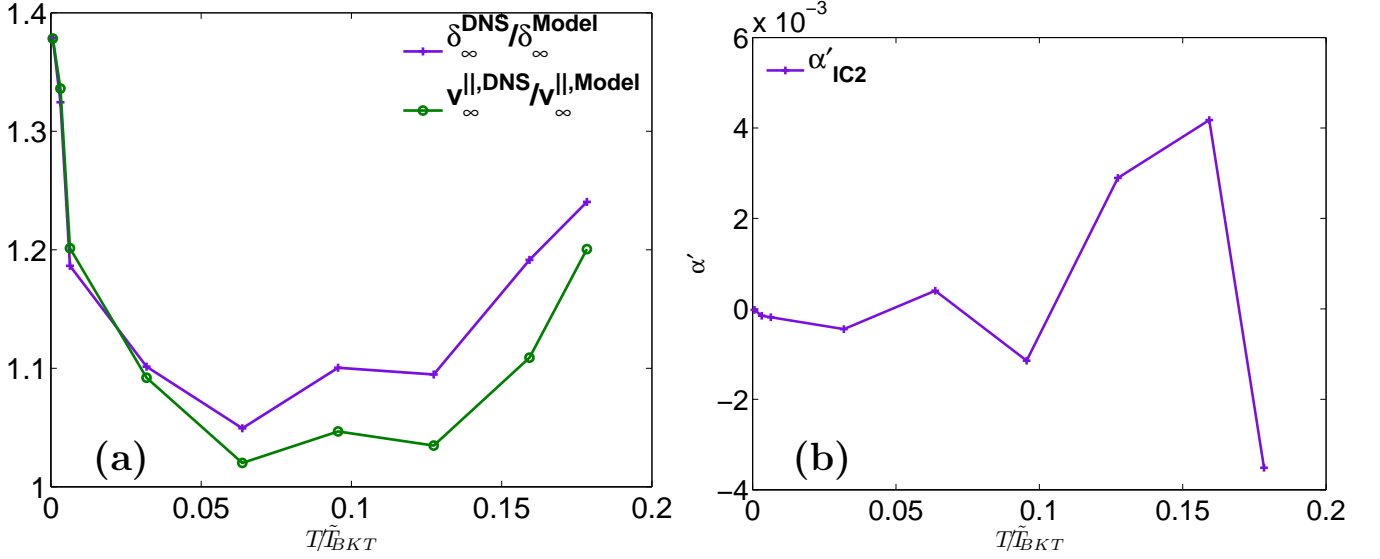


FIG. 5. Plots of the (a)  $\delta_{\infty}^{\text{DNS}}/\delta_{\infty}^{\text{Model}}$  and  $v_{\infty}^{\text{DNS}}/v_{\infty}^{\text{Model}}$  versus  $T/\tilde{T}_{BKT}$ ; (b) mutual friction coefficient  $\alpha'$  versus  $T/\tilde{T}_{BKT}$ , obtained from the DNS runs R1-R9 using the initial configuration IC2.

### 1. Numerical implementation

We use the implicit-Euler method for time stepping in the ARGLE, i.e.,

$$\psi(t + \Delta t) = \frac{\psi(t) + NL(t)\Delta t}{1 - L\Delta t}, \quad (35)$$

where we suppress the spatial argument of  $\psi$ ,  $L = \alpha_0 \nabla^2$ , and  $NL = (\mu - g|\psi|^2)\psi - i\mathbf{u}_{\text{adv}} \cdot \nabla \psi - \frac{\mathbf{u}_{\text{adv}}^2}{4\alpha_0}\psi$ . The field  $\psi$  at the time step  $(n+1)$  is given by

$$\hat{\psi}_{n+1} = \frac{\hat{\psi}_n + \Delta t(\mu - g|\hat{\psi}_n|^2\hat{\psi}_n - i\mathbf{u}_{\text{adv}} \cdot \nabla \hat{\psi}_n - \frac{\mathbf{u}_{\text{adv}}^2}{4\alpha_0}\hat{\psi}_n)}{1 - (-\alpha_0 k^2)\Delta t}. \quad (36)$$

We also use Newton's method to find both the stable and the unstable fixed points of the above equation, which is equivalent to finding  $\psi_*$ , such that

$$F(\psi_*) \equiv \psi_*(t) - \psi_*(t + \Delta t) = 0. \quad (37)$$

Every Newton step requires the solution, for  $\delta\psi$ , of

$$\frac{\delta F}{\delta \psi} \delta \psi = -F(\psi), \quad (38)$$

which we obtain by an iterative bi-conjugate-gradient-stabilized method (BiCGSTAB) [34]. This method uses the direct application of  $[\delta F/\delta \psi]$  over an arbitrary field  $\phi$ , given by

$$\begin{aligned} \frac{\delta F}{\delta \psi} \phi = & \frac{-\Delta t}{1 - L\Delta t} \left[ L\phi + g(2|\psi|^2\phi + \psi^2\phi^*) - i\mathbf{u}_{\text{adv}} \cdot \nabla \phi \right. \\ & \left. - (\mathbf{u}_{\text{adv}}^2/4\alpha_0)\phi \right]. \end{aligned} \quad (39)$$

### 2. Preparation of a translating vortex-antivortex pair: $\psi_{\text{pair}}$

The steps involved in the preparation of  $\psi_{\text{pair}}$  are outlined below:

1. Initialize  $\psi(x, y) = \exp(ix)$  for  $l_{\min} < y < l_{\max}$  and  $\psi(x, y) = 1$  otherwise.
2. Evolve  $\psi$  by using ARGLE, with  $u_{\text{adv}} = 0$ , and allow the vortex-antivortex pair thus generated to contract until it reaches the desired value of the pair length  $d$ .
3. Evolve  $\psi$ , obtained in step 2, by using ARGLE, with  $\mathbf{u}_{\text{adv}} = u\hat{x}$ , so that the contraction of the vortex-antivortex pair stops.
4. Use Newton's method, coupled with BiCGSTAB, to find the exact state of the vortex-antivortex pair for  $\mathbf{u}_{\text{adv}}$  in step 3 above. This Newton method is used to speed up the convergence to the desired solution (because, as the pair solution is a saddle point of Eq. (33), the ARGLE procedure, if used alone, first converges, but finally ends up diverging).

### 3. Preparation of a vortex-lattice: $\psi_{\text{lattice}}$

The steps involved in the preparation of  $\psi_{\text{lattice}}$  are outlined below:

1. Initialize  $\psi = \frac{(\lambda_1 + i\lambda_2)}{A} \tanh(\frac{A}{\sqrt{2}\xi})$ , where  $\lambda_1 = \frac{1}{\sqrt{\gamma_d}} \cos x$ ,  $\lambda_2 = \frac{1}{\sqrt{\gamma_d}} \cos y$ ,  $\gamma_d = 8/(4\pi\alpha_0)$ , and  $A = \sqrt{\lambda_1^2 + \lambda_2^2}$ .

2. Evolve  $\psi$  by using ARGLE, with  $u_{\text{adv},x} = \frac{1}{\gamma_d} \sin(x) \cos(y)$  and  $u_{\text{adv},y} = -\frac{1}{\gamma_d} \cos(x) \sin(y)$ .
3. Evolve  $\psi$ , obtained in step 2, by using ARGLE, followed by Newton-BiCGSTAB, with  $\mathbf{u}_{\text{adv}} = 0$  to find the exact solution.

For more details on the preparation of an assembly of vortices, we refer the reader to Ref. [33].

## V. STOCHASTIC GINZBURG-LANDAU EQUATION (SGLE)

The stochastic Ginzburg-Landau equation (SGLE) is

$$\frac{\partial \psi}{\partial t} = \mathcal{P}_G \left[ \alpha_0 \nabla^2 \psi - g \mathcal{P}_G[|\psi|^2] \psi + \mu \psi - i \mathbf{v}_n \cdot \nabla \psi + \zeta(\mathbf{x}, t) \right], \quad (40)$$

where  $\psi$  is the wave function,  $g$  the interaction strength,  $\mu$  the chemical potential, and  $\mathbf{v}_n$  the counterflow velocity.  $\zeta$  is a Gaussian white noise with

$$\langle \zeta(\mathbf{x}, t) \rangle = 0, \quad (41)$$

$$\langle \zeta(\mathbf{x}, t) \zeta^*(\mathbf{x}', t') \rangle = D \delta(\mathbf{x} - \mathbf{x}') \delta(t - t'), \quad (42)$$

and  $D = 1/(2\alpha_0\beta)$ , where  $\beta = 1/(k_B T)$  (we set the Boltzmann constant  $k_B = 1$ ).

### 4. Numerical implementation

We solve the SGLE (40) along with the following, ad-hoc equation

$$\frac{d\mu}{dt} = -\frac{\nu_N}{\mathcal{A}} (N - N_{av}), \quad (43)$$

to control the number of particles  $N$ ; the parameter  $N_{av}$  controls the mean value of  $N$ ; and  $\nu_N$  governs the rate at which the SGLE equilibrates.

The spatial Fourier-transform of Eq. (40) gives

$$\frac{d\hat{\psi}}{dt} = -\alpha_0 k^2 \hat{\psi} - g \widehat{|\psi|^2 \psi} + \mu \hat{\psi} - i \widehat{\mathbf{v}_n \cdot \nabla \psi} + \hat{\zeta}, \quad (44)$$

where we have omitted the Galerkin projector  $\mathcal{P}_G$  for notational simplicity. We solve the SGLE by using a pseudospectral method with periodic boundary conditions in space and an implicit-Euler scheme, with time step  $\Delta t$ , for time marching. The discrete versions of Eqs. (43) and (44) are

$$\mu_{n+1} = \mu_n - \Delta t \frac{\nu_N}{\mathcal{A}} (N_n - N_{av}) \quad (45)$$

and

$$\hat{\psi}_{n+1} = \frac{\hat{\psi}_n + \Delta t (-g \widehat{|\psi_n|^2 \psi_n} - i \widehat{\mathbf{v}_n \cdot \nabla \psi_n})}{1 + (\alpha_0 k^2 - \mu_n) \Delta t} + dW_\zeta, \quad (46)$$

where  $dW_\zeta = \sqrt{D} (d\mathcal{A})^{-1/2} \eta_i \sqrt{dt}$ , with  $d\mathcal{A} = \Delta x \Delta y$  and  $\eta_i$  are random variables that we obtain from a normal distribution with zero mean and unit variance.

## VI. STANDARD RESULTS ON THE BKT TRANSITION

In this and the following Sections, we extend our discussion [12] of the low-temperature, equilibrium properties of a 2D, interacting Bose gas to situations in which there is a nonvanishing counterflow.

We can use the heuristic, energy-entropy argument to obtain a rough estimate of the BKT transition temperature  $T_{\text{BKT}}$  [12, 15]. In the XY model, this transition is studied by using the Hamiltonian

$$H_{XY} = -J \sum_{\langle i, j \rangle} \cos(\theta_i - \theta_j), \quad (47)$$

where  $\langle i, j \rangle$  denotes nearest-neighbor pairs of sites, on a 2D square lattice,  $J$  is the nearest-neighbor exchange coupling, and  $(\theta_i - \theta_j)$  is the angle between the nearest-neighbor, XY spins on sites  $i$  and  $j$ . In the continuum limit, the above Hamiltonian becomes, to lowest order in spatial gradients,

$$H_{XY} = \frac{J}{2} \int d^2 x (\nabla \theta(x))^2. \quad (48)$$

By comparing Eq. (48) with the kinetic-energy term in the energy, we find that

$$J = \frac{|\langle \psi \rangle|^2 \hbar^2}{m} = \frac{\rho \Gamma^2}{(2\pi)^2}, \quad (49)$$

where  $\Gamma$  denotes the Onsager-Feynman quantum of velocity circulation  $\Gamma = 4\pi\hbar/2m = \hbar/m = \kappa$ . A rough estimate for the BKT transition temperature  $T_{\text{BKT}}$  is given below:

$$\tilde{T}_{\text{BKT}} = \frac{\pi J}{2k_B} = \frac{\pi |\langle \psi \rangle|^2 \hbar^2}{2mk_B} = \frac{\rho \Gamma^2}{8\pi k_B}, \quad (50)$$

here  $\tilde{T}_{\text{BKT}}$  denotes the estimate for  $T_{\text{BKT}}$  that follows from an energy-entropy argument [12].

## VII. LOW-TEMPERATURE THERMODYNAMICAL COMPUTATIONS WITH COUNTERFLOWS

We now develop an analytical framework, which is valid at low-temperatures  $T \ll T_{\text{BKT}}$ , that can be used to test some of the results of our DNS runs in the region of complete thermalization. We calculate the equilibrium thermodynamic functions for a weakly-interacting, 2D Bose gas, in the grand-canonical ensemble. In the grand-canonical ensemble the probability of a given state is

$$\mathbb{P} = \frac{1}{\Xi} e^{-\beta(H - \mu N - \mathbf{w} \cdot \mathbf{P})}, \quad (51)$$

where  $\Xi$  is the grand partition function,  $\beta$  the inverse temperature,  $\mu$  the chemical potential,  $N$  the number



of bosons, and  $\mathbf{P}$  the momentum. The grand-canonical potential is

$$\Omega = -\beta^{-1} \log(\Xi); \quad (52)$$

and the mean energy  $E$  and number of particles  $N$  are

$$N = -\frac{\partial \Omega}{\partial \mu}, \quad (53a)$$

$$\mathbf{P} = -\frac{\partial \Omega}{\partial \mathbf{w}}, \quad (53b)$$

$$E = \frac{\partial \Omega}{\partial \beta} + \mu N + \mathbf{w} \cdot \mathbf{P}. \quad (53c)$$

We adapt to 2D the 3D study of Ref. [11], expand  $\psi$  in terms of Fourier modes  $A_{\mathbf{k}}$ , and obtain  $\Omega$  as the sum of the saddle-point part  $\Omega_{sp}$  and  $\Omega_Q$ , the deviations from the saddle point that are quadratic in  $A_{\mathbf{k}}$ . We write  $\Omega = \Omega_{sp} + \Omega_Q$ , where  $\Omega_{sp} = -\mathcal{A}\mu^2/2g$  and

$$\begin{aligned} \Omega_Q = & -\frac{\mathcal{A}}{2\pi\beta\hbar^2} \int_0^{p_{\max}} \left( \log\left(\frac{2m}{\beta\sqrt{p^4 + 4m\mu^2}}\right) \right. \\ & \left. + \frac{2m^2w^2(5p^2 + 6m^2w^2 + 20m\mu)}{15(p^2 + 4m\mu)^2} \right) p dp, \end{aligned} \quad (54)$$

where  $\mathbf{w} = w\hat{\mathbf{x}}$ . We can also calculate the condensate depletion  $\delta N$ , where the particle number  $N = N_0 + \delta N$ , and  $N_0$  is the number of particles in the  $k = 0$  mode as follows:

$$\delta N = \int_0^{p_{\max}} \frac{mp\mathcal{A} \left( p^{-2} + \frac{1}{p^2 + 4m\mu} \right)}{2\pi\beta\hbar^2} dp + \mathcal{O}(w^2). \quad (55)$$

The integrals in Eqs. (54) and (55) can be performed analytically, but, in contrast to the 3D case where the primitives are zero at  $p = 0$ , the 2D primitive for  $\Omega_{ph}$  is finite at  $p = 0$ ; and for  $\delta N$  it is infra-red (I.R.) divergent. By subtracting the I.R. finite and divergent terms from  $\Omega_Q$  and  $\delta N$ , respectively, we get the following expressions, in 2D, in the thermodynamic limit  $\mathcal{A} \rightarrow \infty$ :

$$\begin{aligned} \Omega = & -\frac{\mu^2\mathcal{A}}{2g} - \frac{p_{\max}^2\mathcal{A}}{4\pi\beta\hbar^2} + \frac{m\mu\mathcal{A}\log(1 + \frac{p_{\max}^2}{4m\mu})}{2\pi\beta\hbar^2} \\ & - \frac{p_{\max}^2\mathcal{A}\log(\frac{2m}{\beta\sqrt{p_{\max}^4 + 4m\mu p_{\max}^2}})}{4\pi\beta\hbar^2} - \frac{m^2w^2\mathcal{A}\log(1 + \frac{p_{\max}^2}{4m\mu})}{6\pi\beta\hbar^2} \\ & + \frac{m^3w^4p_{\max}^2\mathcal{A}}{20\pi\mu\beta\hbar^2p_{\max}^2 + 80\pi m\mu^2\beta\hbar^2} \end{aligned} \quad (56)$$

and

$$\delta N = m\mathcal{A} \frac{\log(1 + \frac{p_{\max}^2}{4m\mu}) + \log(\frac{p_{\max}^2\mathcal{A}}{\hbar^2})}{4\pi\beta\hbar^2} + \mathcal{O}(w^2). \quad (57)$$

By using the thermodynamic relations Eq. (53), we obtain

$$N = \frac{\mu\mathcal{A}}{g} - \frac{m\mathcal{A}\log(1 + \frac{p_{\max}^2}{4m\mu})}{2\pi\beta\hbar^2} + \mathcal{O}(w^2), \quad (58)$$

$$E = \frac{\mu^2\mathcal{A}}{2g} + \frac{p_{\max}^2\mathcal{A}}{4\pi\beta\hbar^2} - \frac{m\mu\mathcal{A}\log(1 + \frac{p_{\max}^2}{4m\mu})}{2\pi\beta\hbar^2} + \mathcal{O}(w^2), \quad (59)$$

and

$$P_x = m^2w\mathcal{A} \frac{\log(1 + \frac{p_{\max}^2}{4m\mu})}{3\pi\beta\hbar^2} + \mathcal{O}(w^3). \quad (60)$$

The expression for  $P_x$  is different from the one that can be derived from the density corresponding to the condensate depletion  $m w \delta N$ ; this allows us to define  $\rho_n = P_x/(w\mathcal{A})$ .

## VIII. LOW-TEMPERATURE RESULTS AT A GIVEN DENSITY

We next determine the chemical potential  $\mu$ , which fixes the total density  $\rho = mN/\mathcal{A}$  at a given value, by solving the equation

$$\rho - \frac{m\mu}{g} + \frac{m^2\log(1 + \frac{p_{\max}^2}{4m\mu})}{2\pi\beta\hbar^2} = 0; \quad (61)$$

at  $\beta = \infty$ , i.e., zero temperature (subscript 0) we obtain

$$\mu_0 = \frac{g\rho}{m}; \quad (62)$$

to order  $\beta^{-1}$  we get

$$\mu = \mu_0 + \delta\mu, \quad (63)$$

where

$$\delta\mu = \frac{mg(4g\rho^2 + \rho p_{\max}^2)\log(1 + \frac{p_{\max}^2}{4g\rho})}{m^2p_{\max}^2 + 2\pi\beta\hbar^2\rho p_{\max}^2 + 8\pi\beta\hbar^2g\rho^2}. \quad (64)$$

We insert  $\mu$  from Eq. (63) into Eq. (57), define the change in density  $\delta\rho = m\delta N/\mathcal{A}$ , use the energy  $E$  from Eq. (59), and then expand to order  $\beta^{-1}$  to obtain

$$\delta\rho = \frac{m^2 \left( \log(1 + \frac{p_{\max}^2}{4g\rho}) + \log(\frac{p_{\max}^2\mathcal{A}}{\hbar^2}) \right)}{4\pi\beta\hbar^2}, \quad (65)$$

and

$$E = \frac{g\rho^2\mathcal{A}}{2m^2} + \frac{p_{\max}^2\mathcal{A}}{4\pi\beta\hbar^2}. \quad (66)$$

We use Eq. (60) and the definition  $\rho_n = P_x/(w\mathcal{A})$  to obtain

$$\rho_n = \frac{m^2\log(1 + \frac{p_{\max}^2}{4g\rho})}{3\pi\beta\hbar^2}. \quad (67)$$

By using Eq. (50) and  $\rho = m |\langle \psi \rangle|^2$ , we obtain

$$\tilde{\beta}_{\text{BKT}} = \frac{1}{k_B \tilde{T}_{\text{BKT}}} = \frac{2m^2}{\pi\rho\hbar^2}, \quad (68)$$

which we can use along with Eq. (65) to relate the condensate relative depletion  $\delta\rho/\rho$  to  $\beta/\tilde{\beta}_{\text{BKT}}$ , where  $\beta = 1/(k_{\text{B}}T)$  and  $k_{\text{B}}$  is the Boltzmann constant, as given below:

$$\frac{\delta\rho}{\rho} = \frac{\tilde{\beta}_{\text{BKT}}}{8\beta} \log \left( \frac{p_{\text{max}}^2 \left( 1 + \frac{p_{\text{max}}^2}{4g\rho} \right) \mathcal{A}}{\hbar^2} \right). \quad (69)$$

Similarly, the normal-fluid density fraction is

$$\frac{\rho_n}{\rho} = \frac{\tilde{\beta}_{\text{BKT}}}{6\beta} \log \left( 1 + \frac{p_{\text{max}}^2}{4g\rho} \right). \quad (70)$$

We use this low-temperature result Eq. (69) to estimate the inverse-temperature scale  $\beta_{\text{BKT}}$ , at which the depletion of the  $k = 0$  condensate mode becomes significant for a finite-size system with  $N_c^2$  collocation points (which fixes the maximum momentum  $p_{\text{max}}$ ); in particular, we can solve Eq. (69), for  $\delta\rho/\rho = 1$ , to obtain

$$\frac{\beta_{\text{BKT}}}{\tilde{\beta}_{\text{BKT}}} = \frac{1}{8} \log \left( \frac{p_{\text{max}}^2 \left( 1 + \frac{p_{\text{max}}^2}{4g\rho} \right) \mathcal{A}}{\hbar^2} \right). \quad (71)$$

By making the replacements that correspond to defining  $\hbar$ ,  $m$ , and  $g$  in terms of  $c$  and  $\xi$ ,  $p_{\text{max}} \rightarrow \hbar k_{\text{max}}$ ,  $\hbar \rightarrow \sqrt{2}cm\xi$ , and  $g \rightarrow c^2m^2/\rho$ , we can rewrite Eq. (69), Eq. (70), and Eq. (71) as

$$\frac{\delta\rho}{\rho} = \frac{\tilde{\beta}_{\text{BKT}}}{8\beta} \log \left( k_{\text{max}}^2 \mathcal{A} \left( 1 + \frac{k_{\text{max}}^2 \xi^2}{2} \right) \right), \quad (72)$$

$$\frac{\rho_n}{\rho} = \frac{\tilde{\beta}_{\text{BKT}}}{3\beta} \log \left( 1 + \frac{k_{\text{max}}^2 \xi^2}{2} \right), \quad (73)$$

and

$$\frac{\beta_{\text{BKT}}}{\tilde{\beta}_{\text{BKT}}} = \frac{1}{8} \log \left( k_{\text{max}}^2 \mathcal{A} \left( 1 + \frac{k_{\text{max}}^2 \xi^2}{2} \right) \right), \quad (74)$$

respectively.

- 
- [1] W. F. Vinen, Phys. Rev. B **61**, 1410 (2000).
  - [2] L. Skrbek and K. R. Sreenivasan, Phys. Fluids **24**, 011301 (2012).
  - [3] N. G. Berloff, M. Brachet, and N. P. Proukakis, Proc. Natl. Acad. Sci. USA **111**, 4675 (2014).
  - [4] C. F. Barenghi, V. S. Lvov, and P.-E. Roche, Proc. Natl. Acad. Sci. USA **111**, 4683 (2014).
  - [5] N. P. Proukakis and B. Jackson, J. Phys. B: At. Mol. Opt. Phys. **41**, 203002 (2008).
  - [6] R. J. Donnelly, *Quantized vortices in helium II*, Vol. 2 (Cambridge University Press, 1991).
  - [7] I. M. Khalatnikov, *An introduction to the theory of superfluidity* (WA Benjamin New York, 1965).
  - [8] C. F. Barenghi, R. J. Donnelly, and W. F. Vinen, J. Low Temp. Phys. **52**, 189 (1983).
  - [9] R. J. Donnelly and C. F. Barenghi, J. Phys. Chem. Ref. Data **27**, 1217 (1998).
  - [10] A. Griffin, T. Nikuni, and E. Zaremba, *Bose-condensed gases at finite temperatures* (Cambridge University Press, 2009).
  - [11] G. Krstulovic and M. Brachet, Phys. Rev. E **83**, 066311 (2011).
  - [12] V. Shukla, M. Brachet, and R. Pandit, New J. Phys. **15**, 113025 (2013).
  - [13] G. Boffetta and R. E. Ecke, Annu. Rev. Fluid Mech. **44**, 427 (2012).
  - [14] R. Pandit, P. Perlekar, and S. S. Ray, Pramana **73**, 157 (2009).
  - [15] J. B. Kogut, Rev. Mod. Phys. **51**, 659 (1979).
  - [16] P. Minnhagen, Rev. Mod. Phys. **59**, 1001 (1987).
  - [17] D. J. Thouless, P. Ao, and Q. Niu, Phys. Rev. Lett. **76**, 3758 (1996).
  - [18] G. E. Volovik, Phys. Rev. Lett. **77**, 4687 (1996).
  - [19] C. Wexler, Phys. Rev. Lett. **79**, 1321 (1997).
  - [20] H. E. Hall and J. R. Hook, Phys. Rev. Lett. **80**, 4356 (1998).
  - [21] E. B. Sonin, Phys. Rev. Lett. **81**, 4276 (1998).
  - [22] C. Wexler, D. J. Thouless, P. Ao, and Q. Niu, Phys. Rev. Lett. **80**, 4357 (1998).
  - [23] J. Fuchs, G. Malka, J. C. Adam, F. Amiranoff, S. D. Baton, N. Blanchot, A. Héron, G. Laval, J. L. Miquel, P. Mora, H. Pépin, and C. Rousseaux, Phys. Rev. Lett. **81**, 4275 (1998).
  - [24] See Supplemental Material for the videos and additional figures.
  - [25] V. Shukla, A. Gupta, and R. Pandit, “Homogeneous Isotropic Superfluid Turbulence in Two Dimensions: Inverse and Forward Cascades in the Hall-Vinen-Bekharevich-Khalatnikov model,” <http://arxiv.org/abs/1409.4537>.
  - [26] Equation (4) is normally written in three dimensions (3D). To use it in 2D, it is simplest to use a 2D projection of an infinitely long and straight vortical filament in 3D.
  - [27] N. G. Berloff and A. J. Youd, Phys. Rev. Lett. **99**, 145301 (2007).
  - [28] G. Krstulovic and M. Brachet, Phys. Rev. B **83**, 132506 (2011).
  - [29] B. Jackson, N. P. Proukakis, C. F. Barenghi, and E. Zaremba, Phys. Rev. A **79**, 053615 (2009).
  - [30] M. E. Fisher, M. N. Barber, and D. Jasnow, Phys. Rev. A **8**, 1111 (1973).
  - [31] S. V. Iordanskii, Sov. Phys.-JETP **22**, 160 (1966).
  - [32] S. V. Iordanskii, Zh. Eksp. Teor. Fiz. **49**, 225 (1965).
  - [33] C. Nore, M. Abid, and M. E. Brachet, Phys. Fluids **9**, 2644 (1997).
  - [34] H. A. Van der Vorst, SIAM J. Sci. Stat. Comput. **13**, 631 (1992).